GA–A27951

BIFURCATION TO EXPANDED H-MODE PEDESTAL WIDTH AND HEIGHT WITH LITHIUM AEROSOL INJECTION IN DIII-D

by

R. MAINGI, G.L. JACKSON, D.K. MANSFIELD, T.H. OSBORNE, B.A. GRIERSON, C.P. CHROBAK, A.G. McLEAN, Z. YAN, S.L. ALLEN, D.J. BATTAGLIA, J.A. BOEDO, A.R. BRIESEMEISTER, J.S. deGRASSIE, R.J. GROEBNER, A.W. LEONARD, G.R. McKEE, R.A. MOYER, R. NAZIKIAN, A.L. ROQUEMORE, P.B. SNYDER, and the DIII-D TEAM

OCTOBER 2014

GENERAL ATOMICS

DISCLAIMER

GA–A27951

BIFURCATION TO EXPANDED H-MODE PEDESTAL WIDTH AND HEIGHT WITH LITHIUM AEROSOL INJECTION IN DIII-D

by
R. MAINGI,* G.L. JACKSON, D.K. MANSFIELD,* T.H. OSBORNE, B.A. GRIERSON,*
C.P. CHROBAK,† A.G. McLEAN,‡ Z. YAN,¶ S.L. ALLEN,‡ D.J. BATTAGLIA,*
J.A. BOEDO,† A.R. BRIESEMEISTER,§ J.S. deGRASSIE, R.J. GROEBNER,
A.W. LEONARD, G.R. McKEE,¶ R.A. MOYER,† R. NAZIKIAN,* A.L. ROQUEMORE,*
P.B. SNYDER, and the DIII-D TEAM

This is a preprint of a paper to be submitted for publication in *Phys. Rev. Lett.*

*Princeton Plasma Physics Laboratory, Princeton, New Jersey.
†University of California San Diego, La Jolla, California.
‡Livermore National Laboratory, Livermore, California.
¶University of Wisconsin-Madison, Madison, Wisconsin.
§Oak Ridge National Laboratory, Oak Ridge, Tennessee.

Work supported by
the U.S. Department of Energy
under DE-AC02-09CH11466, DE-FC02-04ER54698,
DE-FG02-07ER54917, DE-FG02-89ER53296, DE-FG02-08ER54999,
DE-AC52-07NA27344, and DE-AC05-00OR22725

GENERAL ATOMICS PROJECT 30200
OCTOBER 2014

GENERAL ATOMICS

Abstract

Lithium injection into the DIII-D tokamak excited a long-lived edge-localized instability that correlated with a rapid doubling of the width of the edge transport barrier region, i.e. the pedestal. This and other profile changes resulted in extended edge-localized mode (ELM) free periods with steady radiated power; the edge pressure and energy confinement increased by 100% and 60% above the ELMY H-mode. These plasmas were limited by onset of giant ELMs. The stability improvement enabling access to improved pedestals is consistent with observed profile changes and ideal MHD calculations.

The overall performance of fusion devices in high-confinement or H-mode [1] has been linked to the achievable values of the plasma pressure at the edge of the plasma, i.e. at the top of the edge transport barrier ("pedestal") [2,3]. The pedestal pressure, in turn, is usually limited by the onset of periodic relaxation oscillations termed edge localized modes (ELMs) [4]. Substantial research in the past decade has demonstrated that onset of large ELMs is observed when magnetohydrodynamic (MHD) stability limits are reached [5-8]; the drive for these instabilities, ballooning and kink/peeling modes, is provided by high edge pressure gradient and/or edge current respectively [9-11], which are linked through the pressure gradient-driven bootstrap current [12].

Peeling-ballooning calculations with, e.g. the ELITE code [10,11], have reproduced the ELM onset operating space in many devices [13]. Because peeling/ballooning modes are driven by the total free energy in the edge barrier region, either a measured value of the pedestal width is used in conjunction with peeling-ballooning calculations, or a multi-constraint model is used to predict pedestal height and width self-consistently [14]. Experimentally the pedestal width in physical space is proportional to device size, and is typically in the range of a few cm, i.e. 3%-5% in normalized minor radius. A similar normalized width, ~4% of normalized radius, has been predicted for ITER [14].

The shape of the pressure profiles near the magnetic separatrix can substantially alter the ELM stability limit. An increase of the stability limit was achieved with inter-discharge evaporative deposition of lithium (Li) on plasma facing components, which reduced the density and pressure in the vicinity of the separatrix, stabilizing ELMs in NST [7,15-17]. In those cases, the peak pressure gradient remained high but shifted radially inward from the separatrix; the discharges exhibited wide and high pressure pedestals, excellent energy confinement, and improved stability to peeling/ballooning modes. The reduction of the recycling source due to the ability of Li to pump deuterium (D) was integral to the density and pressure reduction [18-20]. Fluctuations were substantially reduced in the edge [19]; however, the particle confinement became too good, and the discharges exhibited temporal impurity accumulation and radiated power ramps.

In the remainder of this Letter, we document a bifurcation of the pedestal profiles and improved performance in DIII-D, achieved with injection of small Li particles into the scrape-off layer (SOL). The broadening of the pedestal profiles was correlated with the appearance of intense fluctuations localized in the pedestal region, which reduced the pressure gradient and current near the separatrix, even in reference discharges prior to the ones with Li injection. Herein lies the key differences with the NSTX results mentioned above [19]: fluctuations *increased* in DIII-D, leading to increased particle transport and steady radiated power during the

ELM-free phases. Furthermore recycling reduction was not needed in DIII-D to enhance the edge confinement and stability, which opens up the prospect of using this technique in traditional high recycling devices.

The critical advances reported here are: 1) the discovery of the high performance pedestal correlated with large pedestal width and the edge-localized fluctuations, and 2) demonstration of reproducible access to the high performance pedestal by stimulating the edge fluctuations with Li. This synergistic combination enables access to ELM-free H-mode over a larger range of input power (2.4-4.2 MW) than usually achievable for naturally occurring ELM-free H-mode ($\leq$2 MW in otherwise similar conditions), and with relatively steady radiated power. In reference discharges prior to the ones with Li injection, the natural 15-25 ms ELM cycle timing was largely unaffected by the edge fluctuations, i.e. naturally occurring ELMs would terminate the fluctuations, restoring the pedestal width to typical values. With Li injection, however, these fluctuations were (a) observed more frequently, and (b) their termination by subsequent ELMs was delayed by the presence of Li in the edge. Long ELM-free periods resulted, in which the pedestal pressure and normalized energy confinement increased by up to 100% and 60% respectively, relative to the ELMy phase of the discharge. The giant ELMs that terminated the ELM-free phases are consistent with ideal stability limits, at substantially higher pedestal pressure than in the reference no-Li ELMy discharges. Experiment details are now described.

Figure 1 compares the time evolution of a reference DIII-D ELMy H-mode discharge with a similar discharge using Li injection. The discharge parameters were plasma current I_p = 1.2 MA, toroidal field on-axis B_t = 2.0 T, auxiliary heating with neutral beams (P_{NBI}) ~ 2.4 MW, in a lower single-null configuration. Lithium powder consisting of ~ 44 μm spheres was dropped into the upper SOL from t = 2.0 s to t = 3.0 s at 1.3×10^{21} atoms/s (6.5×10^5 spheres/s), with a simple device [21]. This method of Li injection shares characteristics with an aerosol, similar to the laser-based system used in TFTR [22]. For reference the typical electron inventory in these discharges was ~ 10^{21}. Panel (a) shows the rise in edge Li density in the Li-enhanced discharge, followed by a gradual decay after t = 3.0 s. Prior to Li injection the reference and Li-enhanced discharges had ordinary "Type 1" ELMs ["spikes" in panels (d,e)] with frequency ~ 100 Hz. Several ELM-free periods were observed in the Li-enhanced discharge both during and after Li injection. Higher injection rates of 4×10^{21} Li atoms/s triggered H-L transitions after only a few hundred ms, while a lower rate ~ 7×10^{20} Li atoms/s created only short (<20 ms duration), frequent ELM-free periods. Note that the baseline D_α level between ELMs in panels (d,e), indicative of the level of quasi-steady recycling of D from the plasma-facing components, did not decrease, in contrast to experiments on other devices. The radiated power showed little evolution with the application of Li [panel (f)]; the normal radiated power spikes during ELMs were observed. Even during the ELM-free phases, there was no evidence of temporal ramping, which is usually associated with impurity accumulation. The overall energy confinement time normalized to the $ITER_{98pby2}$ H-mode scaling law [23] increased from ~ 1.3 up to 2 during the ELM-free phases [panel (g)].

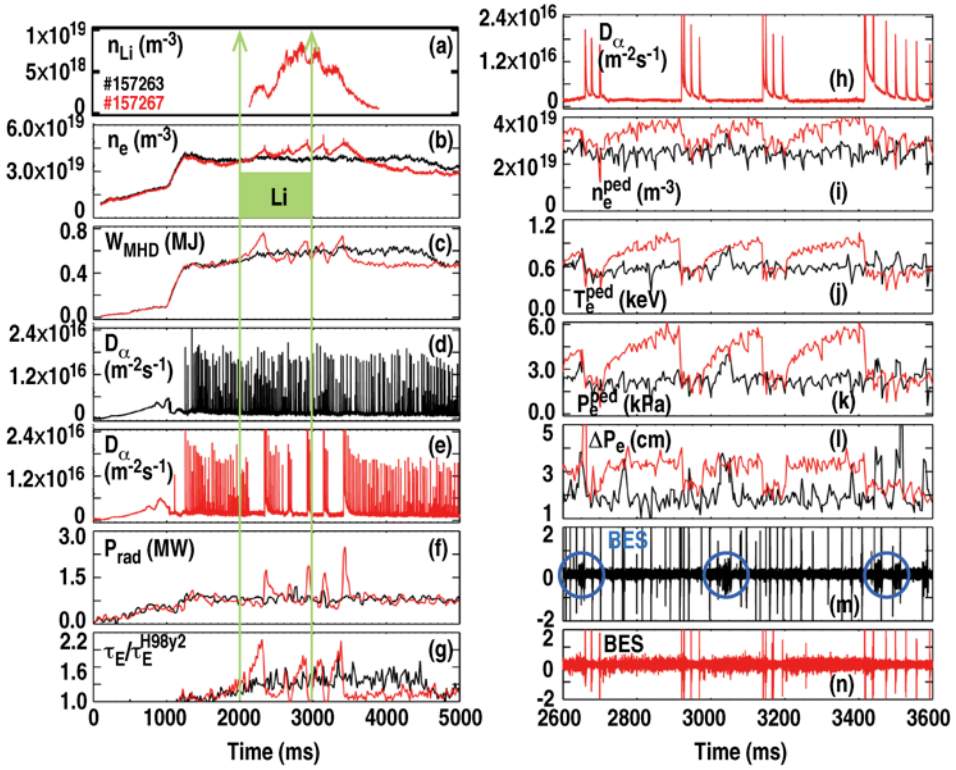

Fig. 1. Time evolution of a reference ELMy discharge (#157263), and a Li-enhanced discharge (#157267) with ELM-free periods in DIII-D: (a) edge Li density n_{Li} from charge exchange recombination spectroscopy, (b) line average electron density n_e, (c) stored energy W_{MHD}, (d) D_α from reference ELMy, (e) and Li-enhanced discharge, (f) total radiated power, (g) energy confinement relative to ITER98 scaling, (h) expanded time base: D_α from Li-enhanced discharge, (i) pedestal n_e height, (j) pedestal T_e height (k) pedestal P_e height, (l) pedestal P_e width, and fluctuation signals from BES (m,n). Vertical lines (LHS) indicate time of lithium injection, and circles in panel (m) indicate occurrences of enhanced fluctuations in reference discharge, becoming nearly steady with Li [panel (n)].

The edge electron density, temperature and pressure (n_e, T_e, P_e) profile heights and P_e profile width, which are obtained from fits to the Thomson scattering data with a commonly used modified hyperbolic tangent function [24], are shown for the same discharges on an expanded time base in panels (h-l). It can be seen that during the ELM-free phases in the Li-enhanced discharge, the P_e pedestal widths from individual profiles increased on average by about and 70%; shorter duration phases with profile broadening can also be seen in the reference discharge. The widths often increased faster than the time between Thomson laser pulses, which occur every 6 ms. In comparison the pedestal heights increased nearly continuously during the ELM-free phases. Thus the average pedestal gradients increased slowly but continuously during the ELM-free periods, with the final peak pressure gradient comparable to the ELMy H-mode peak gradient. Finally panels (m) and (n) show fluctuations from Beam Emission Spectroscopy (BES). Periods of enhanced fluctuations in the reference discharge are circled in panel (m), and the

enhanced fluctuations becoming nearly steady during the ELM-free phases with Li injection [panel (n)].

The long ELM-free periods with Li injection and short ones in reference discharges before Li injection were uniformly correlated with a large increase in edge density fluctuations. These fluctuations were observed in the reference no-Li discharges in 5%-7% of naturally occurring ELM cycles; with Li injection, their onset increased to 10%-15% of ELM cycles. These fluctuations were measured by the BES system, which consists of an 8x8 poloidal/radial array with sub-cm spatial resolution in the pedestal region [25]. Figure 2(a) shows the spectrogram for the BES channel in the pedestal region, showing the clear fluctuation enhancement during a typical ELM-free period from a discharge with Li injection. A dramatic increase in the amplitude was observed for frequencies between 40 and 120 kHz, with an apparent frequency spread $\delta f/f \sim 0.4$. Most of this frequency spread, however, originates from rapid, bursting frequency shifts [Fig. 2(b)], both up and down; the mode itself appears quite coherent, e.g. Fig. 2(c). The associated n_e fluctuation peaked at 8% at r/a of 0.92 [Fig. 2(d)], with propagation in the electron drift direction in the lab frame. We note, however, that there is uncertainty of the separatrix location, such that the mode amplitude may indeed peak in the steep-gradient region. This mode will be referred to as a "Bursty Chirping Mode" (BCM). The poloidal wavenumber k_θ of the BCM is ~ 0.5/cm with $k_\theta \rho_s \sim 0.15$-0.2, i.e. in the long wavelength range characteristic of ion-scale turbulence. The timescale of the pedestal expansion correlated with the time scale for growth of this mode on BES. Effects of the BCM on particle transport were indicated by small increases in the D_α light from the divertor accompanying each burst. The mode amplitude did not typically decrease prior to the onset of ELMs, however, indicating that the extra transport provided by the BCM was insufficient to prevent the pedestal from hitting a stability limit, despite the increase in the pedestal width. This is in contrast to the recently discovered semi-coherent fluctuation with a similar wavelength range observed in EAST [26], which appears to drive sufficient transport to avoid ELMs altogether.

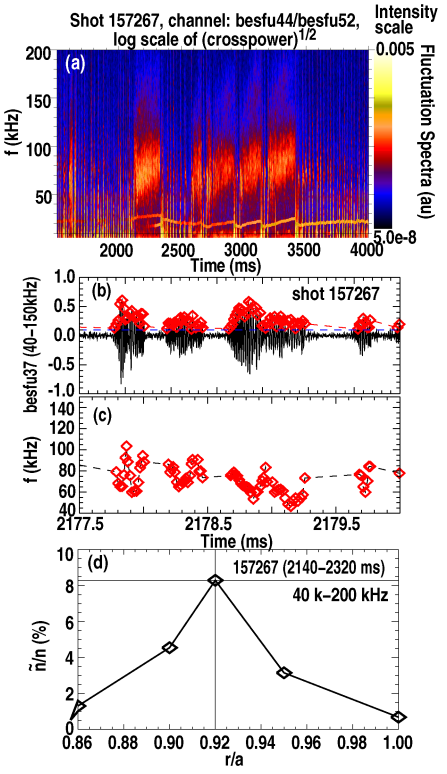

Fig. 2. (a) Spectrogram of BES data from channel in pedestal region for Li-enhanced discharge (#157267); (b) expanded time scale of BES amplitude of an edge channel; (c) frequency of mode, and (d) relative density fluctuation intensity vs. equivalent radius, r/a.

Composite n_e, T_e, P_e, and T_i profiles and their fits from multiple time slices that occurred in the last 20% of the ELM cycle for the reference discharge without the BCM, and from the last 50 ms of a particular ELM-free period from the Li-enhanced discharge with the BCM, are

compared in Fig. 3. The profiles exhibit the steep gradient regions (characteristic of H-modes) near the separatrix, i.e. $\Psi_N = 1$, and a shallow gradient region for $\Psi_N < 0.9$. It can be seen that the electron pedestal widths are substantially larger in the Li-enhanced ELM-free discharge with the BCM, and that the maximum pressure gradient is comparable but shifted inward. In addition, the T_i values are generally higher in the ELM-free discharge, although neither profile exhibited a clear pedestal-like structure.

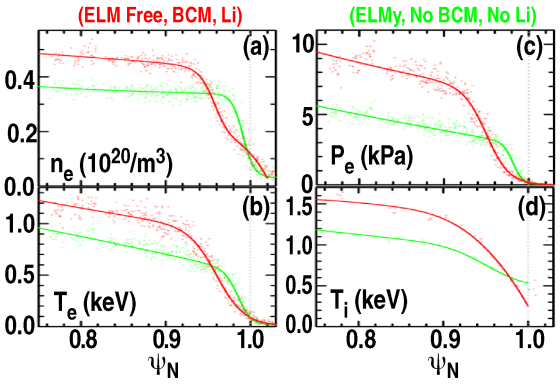

Fig. 3. Comparison of composite radial profiles of (a) n_e, (b) T_e, (c) P_e, and (d) T_i for reference (green - #157263 near 2880 ms) and Li-enhanced (red - #157267 near 3380 ms) discharges. The solid lines are fits to the data (small dots).

Substantial concentrations of Li were measured in the edge and core plasma. Li concentration varied through the ELM-free periods of the discharge shown in Fig. 1 from ~7% of the pedestal n_e for the first ELM-free period ending near 2290 ms, to a maximum of ~16% for the ELM-free period ending near 2880 ms. Carbon, the main intrinsic impurity in DIII-D discharges, varied inversely in concentration to Li, being ~3.2% at 2290 ms and ~1.9% at 2880 ms; the reference ELMy discharge has C concentration ~3%. This compares to a much higher C concentration ~6.7% in a discharge without Li near the end of a similar duration ELM-free period (with reduced P_{NBI} = 2 MW). This inverse dependence of the C concentration on Li suggests that Li acts to exclude other impurities, perhaps contributing to the low radiated power. These high Li concentrations substantially reduced the deuterium density: in the discharge of Fig. 1 at 2880 ms, nearly 45% of the pedestal n_e was accounted for by Li. However the C density was also reduced; thus there was little variation of the total ion pressure in the pedestal region through the Li density variation shown in Fig. 1. The average charge (Z_{eff}) increased from about 1.8-2.0 in the reference ELMy discharge to 2.5 in the Li enhanced discharge. These high Li concentrations contrast with NSTX results [27], in which Li was rarely above 0.1% of the n_e. While the reason for this difference is not understood, edge stability analysis here clearly requires consideration of both C and Li; hence, both species were included in the stability calculations below.

To assess the contribution of changes in pedestal MHD stability to obtaining high pedestal pressure with Li conditioning, ELITE code stability calculations were done for 1) a Li-enhanced discharge with the BCM just before the end of a long ELM-free phase, 2) a reference no-Li ELMy discharge at the same heating power, and 3) a no-Li discharge with heating power reduced to produce ELM-free periods for comparison. The procedure used in these calculations has been previously described [28]. As shown in Fig. 4, equilibria reconstructed from experimental profiles lie near the predicted stability boundary for all three cases. Although there is 1) a modest reduction in the current density driven kink/peeling mode limit due to a shift to

lower unstable toroidal mode number for the wide pedestals obtained with Li, and 2) an increase in the pressure gradient driven ballooning mode limit due to improved diamagnetic stabilization with wide pedestals with Li, these two effects [14] do not play a major role in the overall pedestal pressure increase, as the experimental equilibria for all these cases are similar in normalized current and pressure gradient. Instead the pedestal width expansion observed when the BCM is present and extended with Li injection appears to be the primary cause of the pedestal pressure enhancement within the MHD stability constraint, both by allowing higher pressure at a given pressure gradient, and by allowing a higher dP/dR for a given α when the gradient moves inward to a region of lower safety factor q. Here [10,11] $\alpha = \left[g(\rho) R_0 q^2 \partial\beta / \partial\rho \right]^{max}$, where $\beta = p / \left(B_{t02} / 2\mu_0 \right)$, and $g\rho$ is a geometric factor weakly dependent on radius.

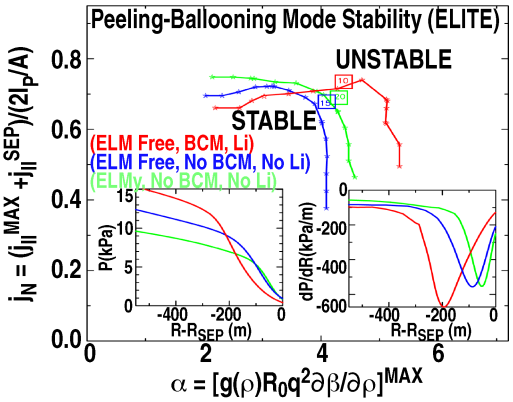

Fig. 4. Comparison of pedestal peeling-ballooning mode stability and pressure profiles just before a Type-I ELM for: (green) a discharge without Li injection at 2.4 MW heating and inter-ELM period of 20 ms, (blue) a discharge without Li injection and 1.4 MW heating near the end of a 240 ms ELM-free period, and (red) a discharge with Li injection and 2.4 MW hearting near the end of a 200 ms ELM-free period. The x-axis is normalized edge pressure gradient, and the y-axis the normalized edge parallel current. Instability is expected above and to the right of the marked stability boundaries (solid curves with stars). Squares mark the location of the experimental equilibrium, and enclose the toroidal mode number of the fastest growing mode. Insets show the pressure profile and its gradient.

The discharges in this Letter can be clearly differentiated from other scenarios with enhanced confinement above H-mode confinement scalings. Quiescent H-mode discharges [29-33] typically have $H_{98y2} \sim 1.0\text{-}1.5$, and have a distinct edge instability known as an Edge Harmonic Oscillation (EHO) that drives particle transport and enables a steady-state pedestal near the stability boundary for current-driven modes [34]. The EHO is a dominant low-n, coherent low frequency ~ 10 kHz mode with higher order harmonics, i.e. clearly distinct from the 70 kHz BCM in Fig. 2. From the literature another instability with similar characteristics is the weakly coherent mode 35,36] from I-mode discharges in Alcator C-mod. Very high confinement or VH-mode [37,38] in DIII-D and the Enhanced Pedestal H-mode [39,40] in NSTX have similar levels of confinement improvement to these discharges, and the presence of long ELM-free periods, but do not have a clear edge instability that correlates with the pedestal broadening.

In summary, the H-mode pedestal width expansion described in this Letter is tied to the presence of the BCM, while Li injection is the key ingredient to both increase the probability that the BCM is destabilized, and extend the ELM cycle duration that otherwise terminates the BCM. The extension of the ELM cycle occurs because of stabilizing profile changes (wider pedestals, pressure gradients moved away from separatrix) and the change in Z_{eff}, which also reduced the edge bootstrap current. This combination of effects resulted in long ELM-free phases at constant

heating power, which eventually reached the (substantially higher pressure) ideal MHD stability limit characteristic of wide pedestals and radially inward shifted profiles. Naturally occurring ELM-free H-modes also exhibit, albeit slower, pedestal width expansion and confinement improvement, but usually suffer from impurity accumulation, and can only be accessed with heating power close to the L-H transition threshold. Li significantly raises the heating power at which long ELM-free periods can be achieved, and the enhanced particle transport from the BCM and/or impurity exclusion by Li ostensibly combine to keep the radiating impurity content low. Moreover, Li injection itself is important: these effects have not been observed with D gas puffing at comparable electron fueling rates. By itself, confinement improvement with Li injection is unsurprising, having been observed in a number of devices [17,41-45]. Nonetheless there is a unique combination of effects in these experiments. A recent experiment on EAST using a nearly identical aerosol injector during plasma discharges found mitigation, and in some cases elimination, of large ELMs, also with steady radiated power, but with no improvement in (relatively modest $H_{98y2} \sim 0.8$) energy confinement times [46]; unfortunately, pedestal profile measurements were unavailable. Relative to the NSTX H-mode results mentioned earlier, there is an additional benefit. The relative insensitivity of baseline D_α emission level to the Li injection in DIII-D means that the improvement in pedestal stability and confinement *does not require* access to a low recycling state. This improves the prospects for applicability in future devices with elevated wall temperatures, which may restrict or eliminate access to low recycling regimes.

References

[1] F. Wagner *et al*., Phys. Rev. Lett. **49** (1982) 1408.

[2] T.H. Osborne *et al*., Plasma Phys. Control. Fusion **40** (1998) 845.

[3] J.E. Kinsey *et al*., Nucl. Fusion **51** (2011) 083001.

[4] H. Zohm Plasma Phys. Control. Fusion **38** (1996) 105.

[5] P.B. Snyder *et al*., Plasma Phys. Control. Fusion **46** (2004) A131.

[6] S. Saarelma *et al*., Plasma Phys. Control. Fusion **49** (2007) 31.

[7] R. Maingi *et al*., Phys. Rev. Lett. **103** (2009) 075001.

[8] S. Saarelma *et al*., Plasma Phys. Control. Fusion **51** (2009) 035001.

[9] J.W. Connor *et al*., Phys. Plasmas **5** (1998) 2687.

[10] H.R. Wilson *et al*., Phys. Plasmas **9** (2002) 1277.

[11] P.B. Snyder *et al*., Phys. Plasmas **9** (2002) 2037.

[12] O. Sauter, C. Angioni and Y.R. Lin-Liu, Phys. Plasmas **6** (1999) 2834.

[13] P.B. Snyder *et al*., Phys. Plasmas **16** (2009) 056118.

[14] P.B. Snyder *et al*., Nucl. Fusion **51** (2011) 103016.

[15] D.K. Mansfield *et al*., J. Nucl. Mater. **390-391** (2009) 764.

[16] D.P. Boyle *et al*., Plasma Phys. Control. Fusion **53** (2011) 105011.

[17] R. Maingi *et al*., Phys. Rev. Lett. **107**, 145004 (2011).

[18] J.M. Canik *et al*., J. Nucl. Mater. **415**, S409 (2011).

[19] J.M. Canik *et al*., Phys. Plasmas **18**, 056118 (2011).

[20] R. Maingi *et al*., Nucl. Fusion **52**, 083001 (2012).

[21] D.K. Mansfield *et al*., Fusion Eng. Design **85** (2010) 890.

[22] D.K. Mansfield *et al*., Nucl. Fusion **41** (2001) 1823.

[23] I.P.B. Team, Nucl. Fusion **39** (1999) 2101.

[24] R.J. Groebner and T.H. Osborne, Phys. Plasmas **5** (1998) 1800.

[25] G.R. McKee Plasma Fusion Res. **2** (2007) S1025.

[26] H.Q. Wang *et al*., Phys. Rev. Lett. **112** (2014).

[27] M. Podestà *et al*., Nucl. Fusion **52** (2012) 033008.

[28] T.H. Osborne *et al*., J. Phys.: Conf. Series **123** (2008) 012014.

[29] KH. Burrell *et al*., Phys. Plasmas **8** (2001) 2153.

[30] C.M. Greenfield *et al*., Phys. Rev. Lett. **86** (2001) 4544.

[31] K.H. Burrell *et al*., Nucl. Fusion **49** (20009) 085024.

[32] A.M. Garofalo *et al*., Nucl. Fusion **51** (2011) 083018.

[33] K.H. Burrell *et al*., Nucl. Fusion **53** (2013) 073038.

[34] P.B. Snyder *et al*., Nucl. Fusion **47** (2007) 961.

[35] D.G. Whyte *et al*., Nucl. Fusion **50** (2010) 105005.

[36] A.E. White *et al*., Nucl. Fusion **51** (2011) 113005.

[37] G.L. Jackson *et al*., Phys. Rev. Lett. **67** (1991) 3098.

[38] T.H. Osborne, K.H. Burrell, and T.N. Carlstrom, Nucl. Fusion **35** (1995) 23.

[39] R. Maingi *et al*., Phys. Rev. Lett. **105** (2010) 135004.

[40] S.P. Gerhardt *et al*., Nucl. Fusion **54** (2014) 083021.

[41] J. Snipes, E.S. Marmar and J.L. Terry, J. Nucl. Mater. **196-198** (1992) 686.

[42] D.K. Mansfield *et al*., Nucl. Fusion **41** (2001) 1823.

[43] R. Majeski *et al*., Phys. Rev. Lett. **97** (2006) 075002.

[44] M. Apicella *et al*., J. Nucl. Mater. **363-365** (2007) 1346.

[45] J. Sánchez *et al*., J. Nucl. Mater. **390-391** (2009) 852.

[46] J.S. Hu Phys. Rev. Lett. submitted (2014).

Acknowledgements

This material is based upon work supported by the U.S. Department of Energy, Office of Science, Office of Fusion Energy Sciences, using the DIII-D National Fusion Facility, a DOE Office of Science user facility, under Awards DE-AC02-09CH11466, DE-FC02-04ER54698, DE-AC05-00OR22725, DE-AC52-07NA27344, DE-FG02-99ER54917 and DE-FG02-89ER53296. DIII-D data shown in this paper can be obtained in digital format by following the links at https://fusion.gat.com/global/D3D_DMP. We gratefully acknowledge the contribution of the DIII-D technical staff. The powder used in this work is trademarked by FMC Corporation as Stabilized Li Metallic Powder® (SLMP®).